



Search for SM Higgs boson production in association with $t\bar{t}$ using no lepton final state

The CDF Collaboration
URL <http://www-cdf.fnal.gov>
(Dated: July 5, 2011)

We search for the Higgs boson produced in association with a $t\bar{t}$. We consider two scenarios of its decay. One is that $t\bar{t}$ decay lepton+jets mode (one t decay bqq' and the other t decay $b\nu$) and the lepton escapes detection. The other is that $t\bar{t}$ decay all hadronic mode (all t decay into bqq'). In both cases we consider that the Higgs boson decays into $b\bar{b}$ but do not explicitly reject other Higgs decay. We use 5.7 fb^{-1} of integrated luminosity of $p\bar{p}$ collision at Tevatron, collected with CDF II detector. We implement neural network to remove dominant backgrounds from QCD multijet production. We check the goodness of our background modeling by comparing data against backgrounds in many control regions, and find good agreement. We select final discriminant variable from different neural network to discriminate the Higgs boson signal from remained backgrounds. Based on the observed data explained by backgrounds without Higgs signals, we set 95% confidence level upper limits on the Higgs boson production cross section. For a Higgs boson mass $M_H = 110 \text{ GeV}/c^2$ the observed(expected) limit is 24.5 (17.8) times the standard model prediction.

Preliminary Results of $t\bar{t}H$ search using 5.7 fb^{-1} in no lepton channel

I. INTRODUCTION

The top quark is the heaviest known elementary particle with its mass $173.3 \pm 1.1 \text{ GeV}/c^2$ [1]. Its large mass suggests that the top quark may play an important role in the electroweak symmetry breaking of the standard model (SM). The production of a Higgs boson in association with a $t\bar{t}$ allows the study of the top Yukawa couplings [2, 3] which plays an important role to understand the nature of mass generation. It is also beneficial to improve low mass Higgs boson search by including new channels which have not been used for the Tevatron combination [4] of Higgs boson search limit.

Even though $t\bar{t}H$ production cross section is very small, its final state has lots of jets, leptons, or missing energy (neutrinos) depending on the decay mode of t and Higgs boson. The large objects on the final state make a distinct signature from background helping a good signal-to-background ratio. However, different decays of t and H give different signatures in the detector making it hard to analyze $t\bar{t}H$ production inclusively using a single final state. Therefore, it is key to study different final states as much as possible for improving the $t\bar{t}H$ search limit.

In this note, we describe a search for Higgs boson production in association with a $t\bar{t}$ in $p\bar{p}$ collisions of $\sqrt{s} = 1.96$ TeV Tevatron collider at Fermilab, collected with the CDF II detector [5]. To avoid overlap with the lepton channel [6], we explicitly exclude events which have high p_T leptons. We consider a scenario of all hadronic decay or lepton+jets decay of $t\bar{t}$ but, an electron or muon escapes detection. The Higgs boson is considered to be $b\bar{b}$ but, we do not explicitly exclude other decay modes.

II. DATA SAMPLE AND EVENT SELECTION

The sample of events used in this measurement is a subset of events selected by a CDF II online selection (trigger), which identifies and records events with at least four jets of transverse energy $E_T > 15 \text{ GeV}$ and a sum E_T of these jets greater than 175 GeV. After trigger selection, events are required to undergo further offline reconstruction, where jets are reconstructed with JETCLUE [7] cone algorithm using a cone radius of $\Delta R = \sqrt{\Delta\phi^2 + \Delta\eta^2} = 0.4$. We define a tight jet to be E_T greater than 15 GeV with $|\eta|$ less than 2.0. To avoid overlaps with lepton channel analysis, we reject events with high p_T electrons or muons. We then select events with the following requirements:

- no high p_T electrons or muons
- leading jet E_T ($E_T^{1st} > 50 \text{ GeV}$)
- 2nd leading jet E_T ($E_T^{2nd} > 40 \text{ GeV}$)
- $H_T = \sum_{\text{tight jets}} E_T + \cancel{E}_T > 300 \text{ GeV}$

We categorize the sample based on the presence of large missing transverse energy (\cancel{E}_T) using \cancel{E}_T significance (\cancel{E}_T^{sig}), where $\cancel{E}_T^{sig} = \cancel{E}_T / \sqrt{\sum E_T}$, to be greater than 2 (\cancel{E}_T +jets channel) or less than 2 (all jets channel). In the \cancel{E}_T +jets channel, we require the following selection additionally

- $\cancel{E}_T^{sig} \geq 2 \text{ GeV}^{1/2}$
- number of tight jets between 5 to 8
- $\text{NN}_{QCD} > 0.8$

while all jets channel have

- $\cancel{E}_T^{sig} < 2 \text{ GeV}^{1/2}$
- number of tight jets between 7 to 11
- $\text{NN}_{QCD1} > 0.9$
- $\text{NN}_{QCD2} > 0.7$

requirements. Number of jets requirements are corresponding to our consideration of each channel which are six jets in the \cancel{E}_T +jets channel and eight jets in the all jets channels. The neural network (NN) output of each sample will be discussed later.

The NN based b tagger [8] uses the track information to tag jets as coming from b quarks. We require at least two tagged jets per event. In both channels, we separate the sample based on number of b -tagged jets as exactly two b -tagged jets (2-tag) and three or more than three b -tagged jets (3-tag) events.

Background events with b tags can arise not only from $t\bar{t}$ but also from QCD multijet and electroweak productions of W bosons associated with heavy flavor jets. However no requirement of charged lepton makes the dominant background caused by QCD multijet production. In order to improve the signal-to-background ratio in this analysis, a NN is trained to identify the kinematic and topological characteristics of SM $t\bar{t}H$ events against data without b -tag requirement which are dominated by QCD multijet production. Below are lists of input variables of this NN.

- \cancel{E}_T^{sig} : The \cancel{E}_T significance defined as $\cancel{E}_T/\sqrt{\Sigma E_T}$.
- $\Delta\phi_{min}$: The minimum difference between the \cancel{E}_T and tight jets in the ϕ angle.
- Aplanarity : Energy and Topology related variables.
- H_T : Sum of the transverse energy of jets and missing energy
- LR_all : Quark gluon likelihood ratio to separate quark jet from gluon jet. Quark gluon likelihood ratio is jet variable so, LR_all is averaged by all of tight jets.
- LR_other : Quark gluon likelihood ratio averaged by tight jets without three leading jets
- E_{T1} : The transverse energy of the leading jet.
- SumEt3 : Sum of the transverse energy of tight jets without two leading jets. Here jets are ordered by E_T
- njets : Number of tight jet
- maxDijet : Maximum invariant mass of two jets.
- minDijet : Minimum invariant mass of two jets.
- maxTrijet : Maximum invariant mass of three jets.
- minTrijet : Minimum invariant mass of three jets.
- E_{T2} : The transverse energy of the 2^{nd} leading jet.
- E_{T3} : The transverse energy of the 3^{rd} leading jet.

The trainings are done separately for \cancel{E}_T +jets and all jets channel. We use first nine input variables for \cancel{E}_T +jets in the list while we use last 12 input variables for all jets channel. We apply the NN to all events and reject large amount of QCD multijet events by selecting high score NN output events which have close kinematics with $t\bar{t}H$ signature. Figure 1 (a) shows this NN output (NN_{QCD}) in the \cancel{E}_T +jets channel using inclusive tagged sample ($b\text{-tag} \geq 1$). We reject the events which have NN_{QCD} less than 0.8. Figure 1 (b) and (c) show this output distribution in signal region separately for 2-tag and 3-tag categories. Figure 2 (a) shows NN output (NN_{QCD1}) in the all jets channel. We reject significant amount of non- $t\bar{t}$ background by using $NN_{QCD1} > 0.9$ which we call Pre-signal region. However, this channel still have significant non- $t\bar{t}$ background due to the dominant QCD multijet production in the Pre-signal region. We then have 2^{nd} stage NN for the further rejection of non- $t\bar{t}$ events. Figure 3 (a) shows 2^{nd} stage NN output (NN_{QCD2}) which we use the events passing NN_{QCD1} selection (Pre-signal events) with 13 input variables from the list. We reject

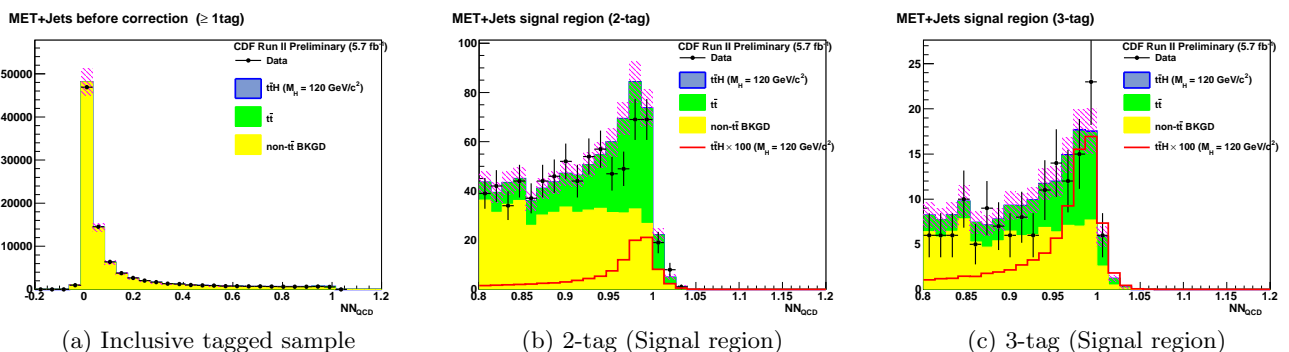


FIG. 1: NN output (NN_{QCD}) of \cancel{E}_T +jets channel to reject QCD multijet events.

TABLE I: Expected number of background and signal events. We assume $M_{\text{top}} = 172.5 \text{ GeV}/c^2$ with 7.0 pb cross section and $M_H = 120 \text{ GeV}/c^2$ with 4.9 fb.

	CDF II Preliminary 5.7 fb ⁻¹			
	2-tag (\cancel{E}_T +jets)	3-tag (\cancel{E}_T +jets)	2-tag (all jets)	3-tag (all jets)
Signal	1.0 ± 0.1	0.8 ± 0.1	0.7 ± 0.1	0.8 ± 0.1
$t\bar{t}$	316.1 ± 43.3	66.6 ± 9.8	120.7 ± 16.5	43.1 ± 6.4
non- $t\bar{t}$	488.9 ± 41.4	98.5 ± 12.6	328.9 ± 35.3	82.7 ± 11.8
Total Expected	806.0 ± 59.8	165.9 ± 16.0	450.3 ± 38.9	126.6 ± 13.4
Observed	756	151	424	133

the events having $\text{NN}_{QCD2} < 0.7$. Figure 3 (b) and (c) shows this NN output (NN_{QCD2}) in the signal region for 2-tag and 3-tag respectively.

We estimate the background b tags based on a per jet parameterization of the b -tagging probability from a background dominant sample. In the \cancel{E}_T +jets, we use the sample containing events with exactly three jets, which have negligible contamination of $t\bar{t}$ and $t\bar{t}H$. For the all jets modeling, we use exactly four jets events. We parameterize the per jet b -tag rate as a function of three jet characteristics. Two variables are same in both channels: jet E_T and the number of good quality charged tracks inside the jet cone. We use the projection of \cancel{E}_T along the jet direction, $\cancel{E}_T^{\text{proj}} = \cancel{E}_T \cos\Delta(\cancel{E}_T, \text{jet})$ for third variable of \cancel{E}_T +jets channel while number of good quality z-vertices of $p\bar{p}$ interaction is used for all jets channel. Due to the presence of $t\bar{t}$ events in samples with higher jet-multiplicity, we extrapolate the b -tagging probability to higher jet-multiplicity events by iteratively removing $t\bar{t}$ content from the sample [9]. We calculate the background b tags for 2-tag and 3-tag samples separately, but a b -tagging correction factor, as described in Ref. [10], is applied to take into account the fact that most of the heavy flavor jets are produced in pairs. Due to the difference of tag probability caused by different sample composition and detector effect from higher jet-multiplicity events, we have reweight number of jets distribution using background dominant samples (low score, less than 0.4, NN_{QCD} or NN_{QCD1}). Due to the imperfect modeling of very low score NN_{QCD} (NN_{QCD1} for all jets), less than 0.05, we do not use those events but, total rate differences in the NN_{QCD} or $\text{NN}_{QCD1} < 0.05$ are used to assign systematic uncertainties of background rate from background modeling. With the background rate estimation procedure described above, we obtain the estimated numbers of background events in Table I. The table also show the estimated $t\bar{t}$ background, with an assumed $t\bar{t}$ production cross section of 7.0 pb at $M_{\text{top}} = 172.5 \text{ GeV}/c^2$, and $t\bar{t}H$ signal, with an assumed $t\bar{t}H$ production cross section of 4.9 fb [3] at $M_H = 120 \text{ GeV}/c^2$. Monte Carlo (MC)-simulated $t\bar{t}$ and $t\bar{t}H$ samples are generated by PYTHIA [12]. We generate different $t\bar{t}H$ samples with M_H between 100 GeV/c^2 and 150 GeV/c^2 .

III. CONTROL REGION

To verify the modeling of background, we test our ability to predict the background in the control regions. The first control region is exactly one b -tag (1-tag) signal region. We request all the other signal requirements without b -tagging. In this region, we expect significant amount of $t\bar{t}$ as well as non- $t\bar{t}$ background. Figure 4 show examples of our estimations in this region. We have very nice agreement in both channels.

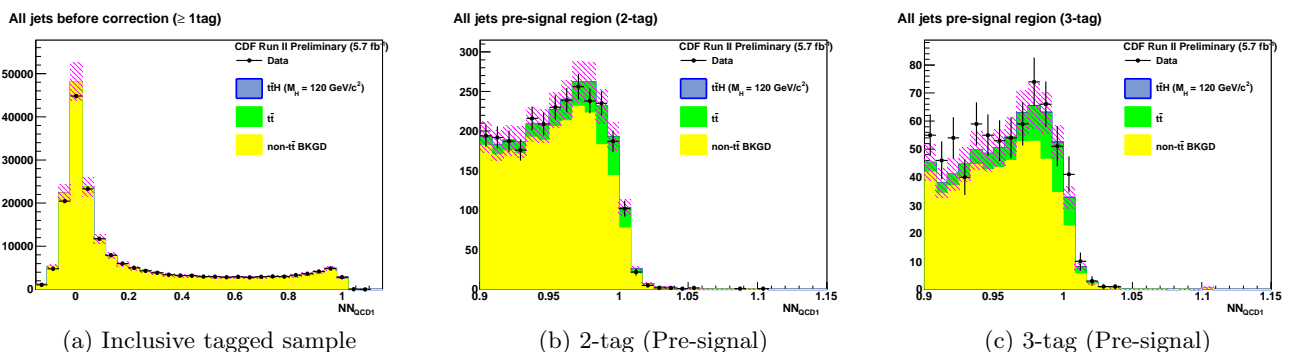


FIG. 2: First stage NN output (NN_{QCD1}) of all jets channel to reject QCD multijet events.

Another control region is the NN_{QCD} in between signal and background regions, where background region ($NN_{QCD} < 0.4$) is used for background modeling. In the \cancel{E}_T +jets channel, we use $0.4 < NN_{QCD} < 0.8$ events as control region. In the all jets channel, we have two control region. One (Control1 region) is $0.4 < NN_{QCD1} < 0.9$ without any requirement of NN_{QCD2} and the other (Control2 region) is $NN_{QCD1} > 0.9 \&\& NN_{QCD2} < 0.7$. Control2 region have relatively larger $t\bar{t}$ contribution than control1 region. Figures 5, 6, and 7 show the examples of validation plots in each control region. Generally, we describe our data with expectation very well in the different control regions which allow us to use our background modeling in the signal region with confidence.

IV. SIGNAL DISCRIMINATION

In the our signal region, the dominant backgrounds are non- $t\bar{t}$ including QCD multijet and electroweak W+jets production and $t\bar{t}$. We study the dynamics of those events to develop a NN with the goal of discriminating the survived background from the $t\bar{t}H$ signals.

Since NN_{QCD} (\cancel{E}_T +jets) and NN_{QCD2} (all jets) have separation power between signals and non- $t\bar{t}$ backgrounds, we train a NN to separate $t\bar{t}$ from $t\bar{t}H$ in each channel separately. We trains a $t\bar{t}H$ signal with $M_H = 120 \text{ GeV}/c^2$ against a $t\bar{t}$ MC with $M_{top} = 172.5 \text{ GeV}/c^2$. We use 13 input variables for each channel with slightly different choice from the list of input variable of QCD NN.

Figure 8 shows the NN output (NN_{Top}) of this training in each channel. Because we train this NN between $t\bar{t}H$ and $t\bar{t}$, discrimination of non- $t\bar{t}$ using NN_{Top} is much poorer than $t\bar{t}$ discrimination. Therefore we choose final discriminant as the multiplication of two NN output, NN_{QCD} (or NN_{QCD2}) $\times NN_{Top}$. Figure 9 show the final discriminants of each category.

V. SYSTEMATIC UNCERTAINTIES

We consider a variety of systematic effects that could change the rate as well as the shape of signals or backgrounds. The rate uncertainty reflect changes to the event yield due to systematic effects while the shape uncertainty reflect changes to the final discriminant template histograms.

Cross section: We use NLO cross section to normalize the events for $t\bar{t}$ and $t\bar{t}H$. The theoretical uncertainties of each calculation, which are 10% in both case, are assigned as systematic uncertainty.

Trigger simulation: For the MC ($t\bar{t}$ and $t\bar{t}H$), we simulate our top multijet trigger using calorimeter trigger tower information. We check our simulation using jet data compared with jet MC sample. The difference between simulation and data are assigned as systematic which is 7% in the rate of $t\bar{t}$ and $t\bar{t}H$.

Luminosity: The uncertainty of luminosity measurement (6%) is assigned as systematic of $t\bar{t}$ and $t\bar{t}H$.

B-tagging scale factor: B-tag scale factor (0.92 ± 0.04) (b -tagging rate difference between data and MC) are applied to b -tagged jet to correct b -tag rates of MC generated events. We applied this scale factor for $t\bar{t}$ and $t\bar{t}H$ in each category

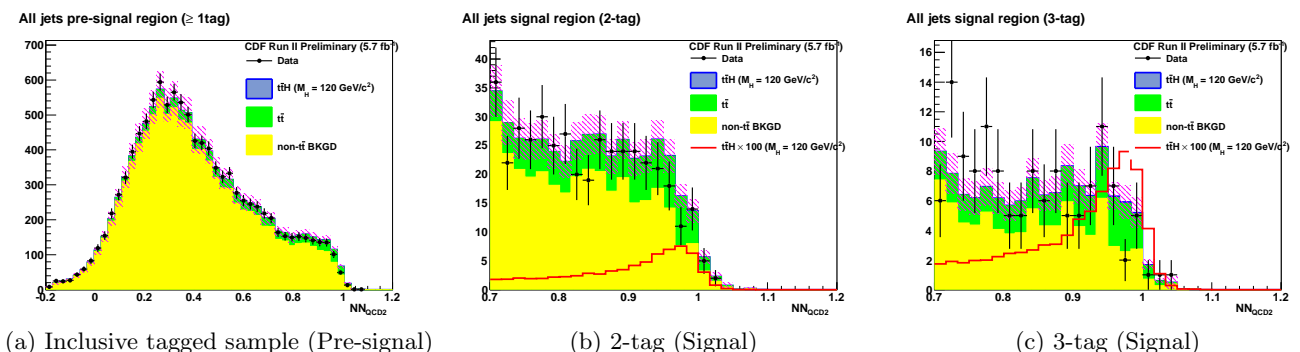


FIG. 3: Second stage NN output (NN_{QCD2}) of all jets channel for further rejection of QCD multijet events.

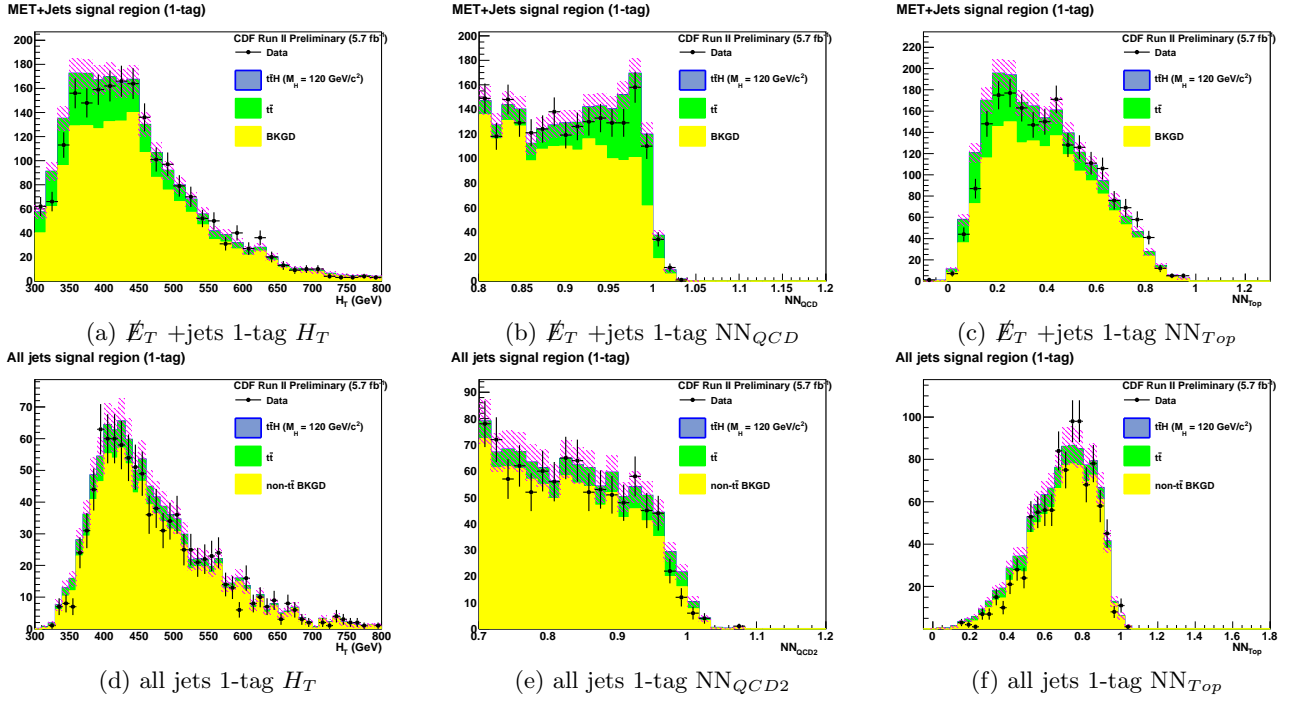


FIG. 4: 1-tag signal region passing all the other cut without b -tagging requirement (Here we request exactly one b tag instead).

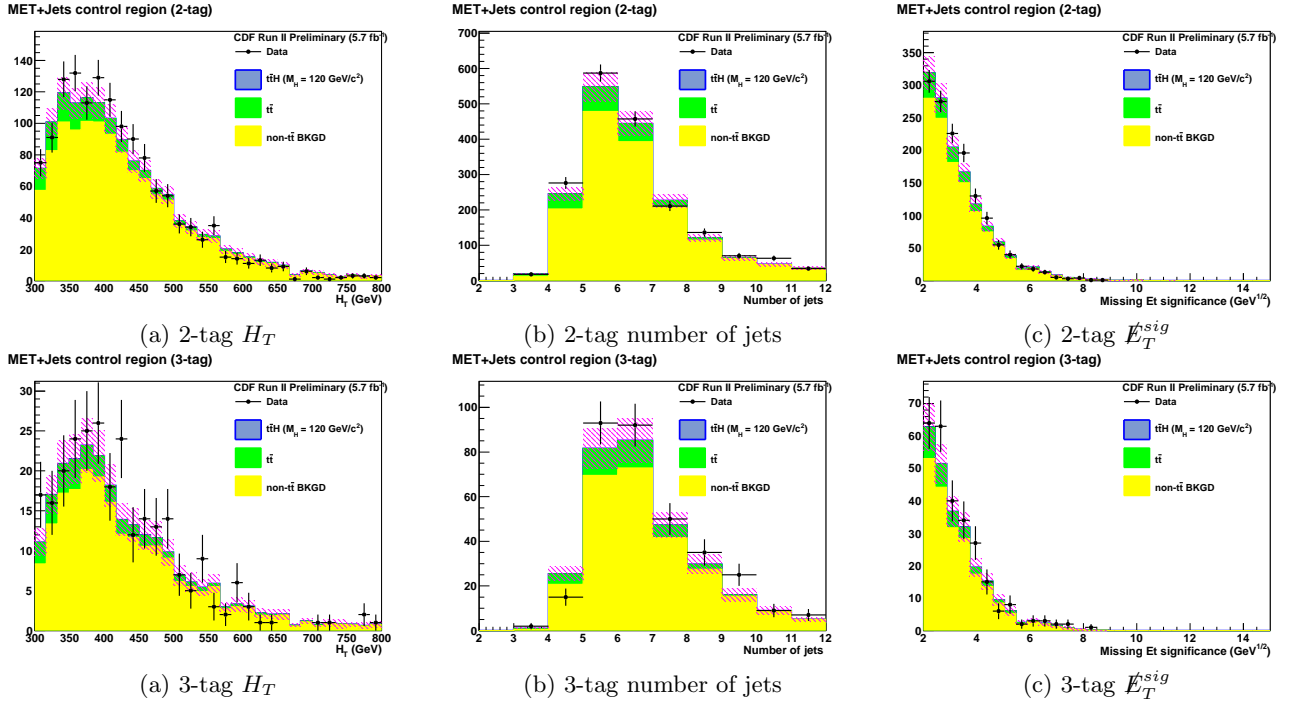


FIG. 5: Example of control region validation in the \cancel{E}_T +jets channel. We require all the other cut without NN_{QCD} selection, number of jets distribution do not have n_{jets} requirement.

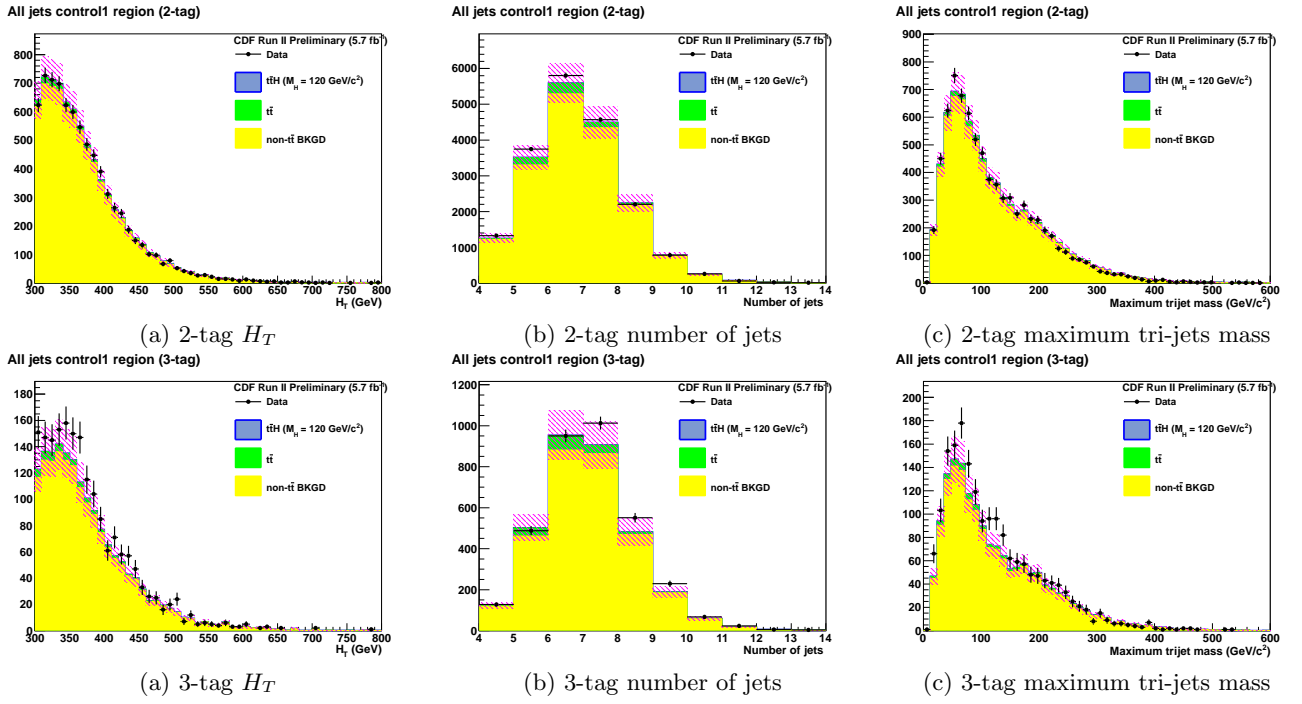


FIG. 6: Examples of control1 region validation in the all jets channel. We require all the other cut without NN_{QCD1} selection, number of jets distribution do not have njets requirement.

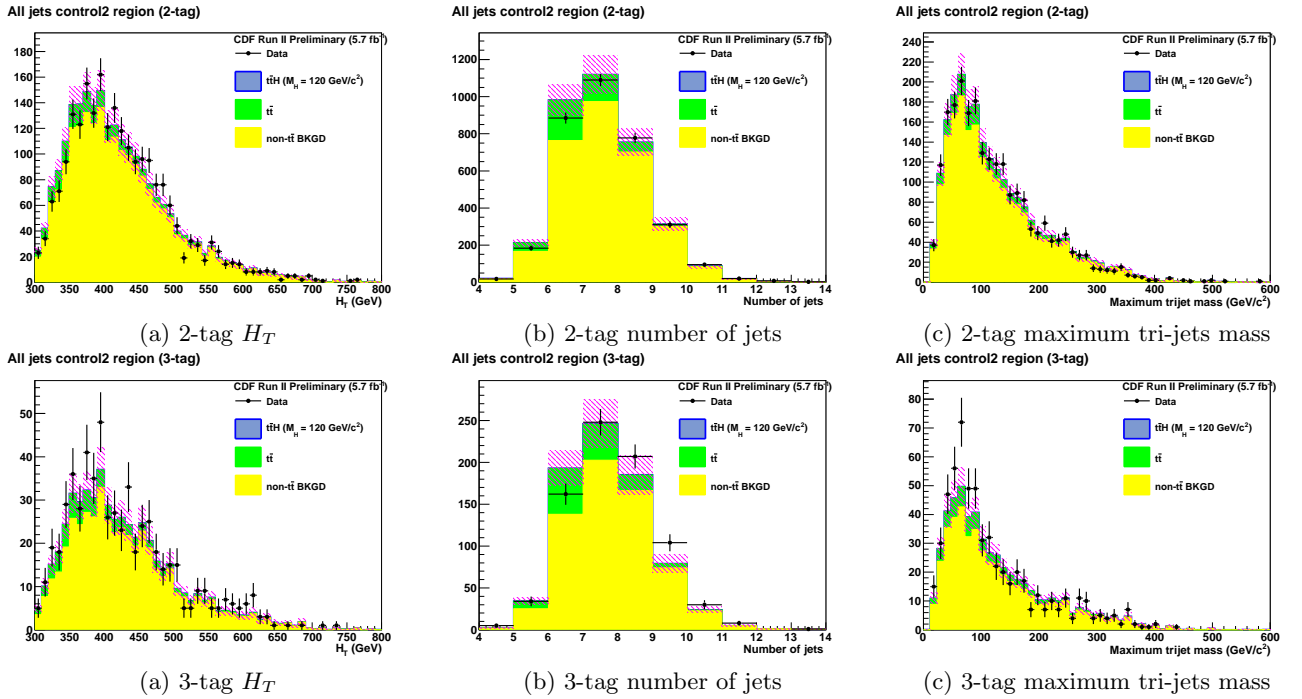


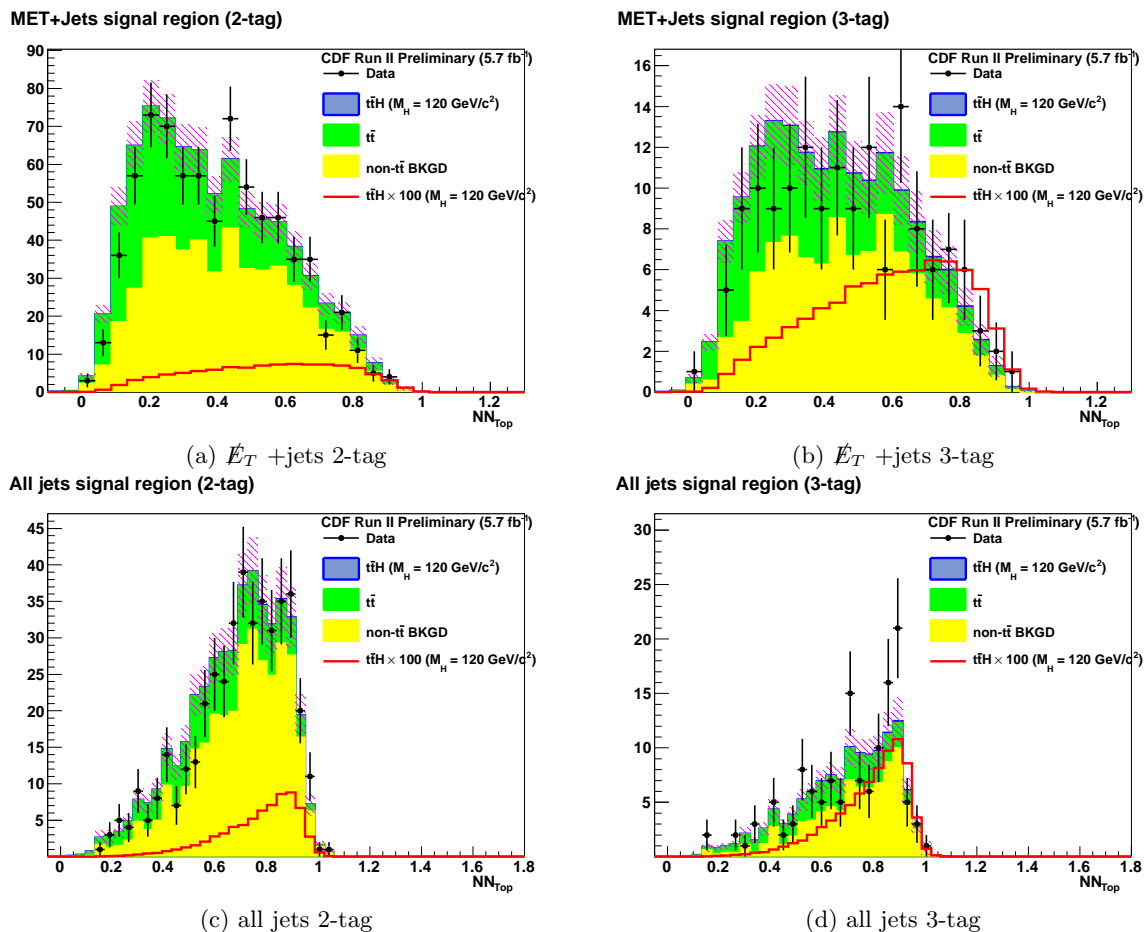
FIG. 7: Examples of control2 region validation in the all jets channel. We require all the other cut without NN_{QCD2} selection, number of jets distribution do not have njets requirement.

TABLE II: Relative systematic uncertainties on the rate are shown. Uncertainties are relative to the rate of each process.

Systematic sources	\cancel{E}_T +jets channel						All jets channel					
	$t\bar{t}H$		$t\bar{t}$		non- $t\bar{t}$		$t\bar{t}H$		$t\bar{t}$		non- $t\bar{t}$	
	2-tag	3-tag	2-tag	3-tag	2-tag	3-tag	2-tag	3-tag	2-tag	3-tag	2-tag	3-tag
Cross section	10%	10%	10%	10%	-	-	10%	10%	10%	10%	-	-
Trigger	7%	7%	7%	7%	-	-	7%	7%	7%	7%	-	-
Luminosity	6%	6%	6%	6%	-	-	6%	6%	6%	6%	-	-
B-Tag Scale Factor	7%	9%	7%	9%	-	-	7%	9%	7%	9%	-	-
JES	2%	3%	11%	13%	-	-	5%	7%	20%	22%	-	-
I/FSR	2%	2%	2%	2%	-	-	2%	2%	2%	2%	-	-
PDF	2%	2%	2%	2%	-	-	2%	2%	2%	2%	-	-
$t\bar{t}b\bar{b}$	-	-	3%	5%	-	-	-	-	3%	6%	-	-
BKGD Modeling	-	-	-	-	6%	6%	-	-	-	-	9%	9%
b -tag Categorization	-	-	-	-	5%	10%	-	-	-	-	5%	10%

and assign the propagated uncertainties as systematic corresponding to approximately 7% for 2-tag and 9% for 3-tag in both $t\bar{t}$ and $t\bar{t}H$ events.

Jet energy scale (JES): We vary the JES of MC generate events within our knowledge [11] within $\pm 1\sigma$ uncertainty. The variation of JES bring not only rate change but also shape change of final discriminant template. We have

FIG. 8: NN output (NN_{Top}) for $t\bar{t}$ separation.

2% (3%) and 11% (13%) of rate uncertainties for $t\bar{t}H$ and $t\bar{t}$ respectively in 2-tag (3-tag) \cancel{E}_T +jets category. In the all jets channel, we have 5% (7%) and 20% (22%) of rate uncertainties for $t\bar{t}H$ and $t\bar{t}$ respectively for 2-tag (3-tag) events.

Initial and Final state radiation: We consider the 2% rate uncertainties from initial and final state radiation uncertainty for $t\bar{t}$ and $t\bar{t}H$.

Parton distribution functions: We consider the rate variation of $t\bar{t}$ and $t\bar{t}H$ from different choice of parton distribution functions. We assign 2% rate uncertainties in both cases.

NLO $t\bar{t}b\bar{b}$ cross section uncertainty: The Ref. [13] shows that $t\bar{t}b\bar{b}$ cross section in the NLO can be different with leading order (LO) estimation as much as twice in the LHC energy scale. Because we use LO MC (pythia), but normalized into NLO cross section, to model the $t\bar{t}$ with all inclusive jets sample, we consider the twice of $t\bar{t}b\bar{b}$ cross section which bring 3-6% rate increasing depending on categories. This uncertainty bring not only rate change of $t\bar{t}$ but also shape change of $t\bar{t}$ histogram. Because we already normalize our LO MC to NLO cross section, we are taking this uncertainty quite conservatively.

Background (non- $t\bar{t}$) rate and shape uncertainty: We consider the uncertainty of non- $t\bar{t}$ background estimation. The uncertainties of background estimation, which are caused by mismatching the rate in $NN_{QCD} < 0.05$ region, are 6% and 9% for \cancel{E}_T +jets and all jets channel respectively. The scale uncertainty of b -tagging categorization also give systematic uncertainty about 5% for 2-tag and 10% for 3-tag in both channels. Because these background rate uncertainties are correlated acrossing each event, we consider the shape change of background template by distorting

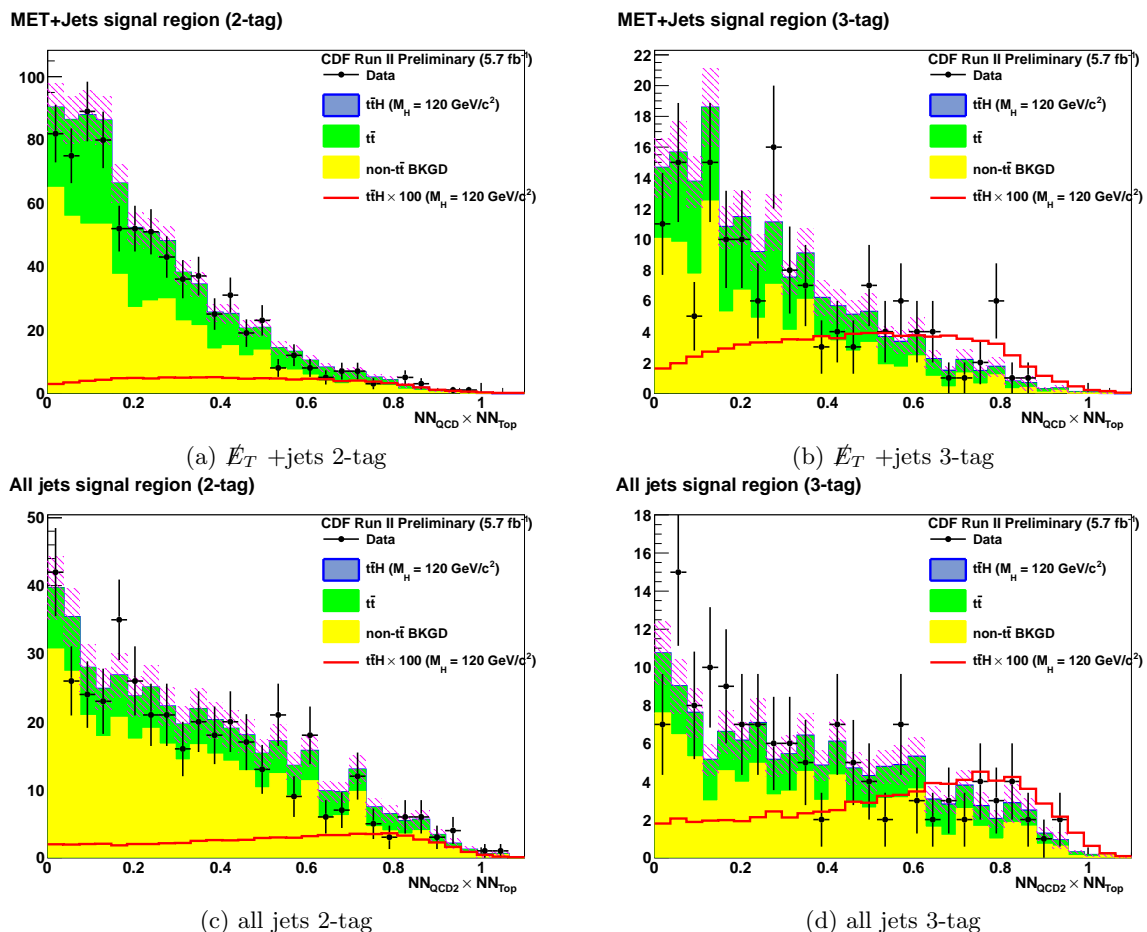


FIG. 9: Final discriminant of $t\bar{t}H$ search

TABLE III: Limit on SM Higgs boson cross section divided by predicted SM cross section using $t\bar{t}H$ production in the \cancel{E}_T +jets and all jets channels

M_H (GeV/ c^2)	CDF II Preliminary 5.7 fb $^{-1}$					Observed Limits
	Expected Limits					
	-2σ	-1σ	Median	1σ	2σ	
100	6.3	10.0	15.2	22.6	32.6	21.5
105	6.9	10.8	16.3	23.8	34.8	23.0
110	7.6	11.7	17.8	26.3	37.7	24.5
115	8.2	13.2	20.2	30.1	43.3	28.1
120	9.7	15.1	22.9	34.2	49.1	31.4
125	11.3	17.5	26.2	39.5	56.9	36.2
130	13.5	20.8	31.5	46.8	66.9	43.6
135	15.4	24.3	36.8	54.6	78.4	48.6
140	18.3	28.9	44.2	65.8	95.6	56.2
145	21.7	35.0	53.4	79.8	114.5	68.1
150	25.2	39.7	60.3	89.9	126.9	72.6

the shape of H_T within its rate uncertainty. We consider the maximum shape change of final discriminant which are caused by increasing and decreasing probability as a function of H_T .

Table II shows summary of systematic uncertainties in relative rate to each process. The JES, $t\bar{t}b\bar{b}$, and non- $t\bar{t}$ background have shape variation in addition.

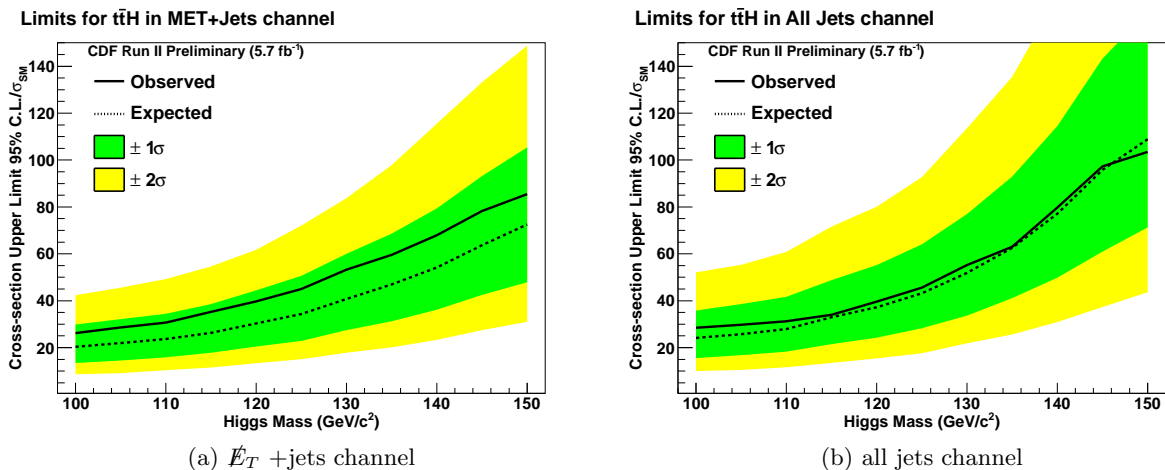


FIG. 10: Limit on SM Higgs boson cross section divided by predicted SM Higgs boson cross section for each channel

VI. RESULTS

We compute the expected limit for standard model Higgs boson cross section in the production associated with a $t\bar{t}$. We build a binned likelihood to extract signal components with gaussian constraints of background normalization within their uncertainties using final discriminant histograms (Fig. 9). The systematic normalizations are incorporated into the likelihood as nuisance parameters. We use MCLIMIT packages [14] for the statistical treatment of limit calculation. Figure 10 show 95% confidence level upper limit of Higgs boson cross section of \cancel{E}_T +jets (a) and all jets (b) channel. Table III and Fig. 11 show the combined limit of two channel together. All the cross sections are ratios with respect to the standard model cross section.

VII. SUMMARY

We have presented a first search of $t\bar{t}H$ signature with no lepton final states. Using 5.7 fb^{-1} of CDF data, we set the 95% confidence level upper limit of standard model Higgs boson cross section as 24.5 (17.8) times the standard model prediction of observed (expected) limit for $M_H = 110 \text{ GeV}/c^2$.

Acknowledgments

We thank the Fermilab staff and the technical staffs of the participating institutions for their vital contributions. This work was supported by the U.S. Department of Energy and National Science Foundation; the Italian Istituto Nazionale di Fisica Nucleare; the Ministry of Education, Culture, Sports, Science and Technology of Japan; the Natural Sciences and Engineering Research Council of Canada; the National Science Council of the Republic of China; the Swiss National Science Foundation; the A.P. Sloan Foundation; the Bundesministerium für Bildung und Forschung, Germany; the Korean World Class University Program, the National Research Foundation of Korea; the Science and Technology Facilities Council and the Royal Society, UK; the Institut National de Physique Nucleaire et Physique des Particules/CNRS; the Russian Foundation for Basic Research; the Ministerio de Ciencia e Innovación, and Programa Consolider-Ingenio 2010, Spain; the Slovak R&D Agency; the Academy of Finland; and the Australian Research Council (ARC).

-
- [1] The Tevatron Electroweak Working Group (CDF and D0 Collaborations), FERMILAB-TM-2466-E, arXiv:1007.3178v1.
 [2] W. Beenakker et al., Phys. Rev. Lett. **87**, 201805 (2001); U. Aglietti et al., arXiv:hep-ph/0612172v2.
 [3] L. Reina and S. Dawson, Phys. Rev. Lett. **87**, 201804 (2001); L. Reina, S. Dawson, and D. Wackerroth, Phys. Rev. D **65**, 053017 (2002).
 [4] The Tevatron Higgs Working Group (CDF and D0 Collaborations), FERMILAB-CONF-11-044-E, arXiv:1103.3233v2.
 [5] D. Acosta et al. (CDF Collaboration), Phys. Rev. D **71**, 032001 (2005).
 [6] S. Lai, Ph.D thesis, CDF public note 9508; CDF Collaboration, CDF note 10548, conference note in preparation.
 [7] F. Abe, et al., Phys. Rev. D **45**, 1448 (1992).

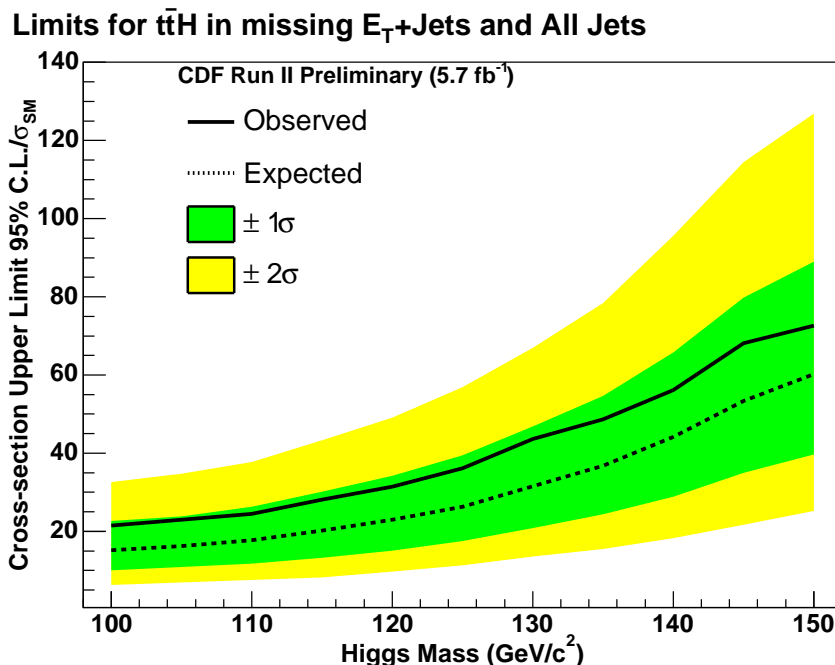


FIG. 11: Limit on SM Higgs boson cross section divided by predicted SM Higgs boson cross section combined with two channels

- [8] CDF Collaboration, CDF Conference note 10311 (2011).
- [9] T. Aaltonen et al. (CDF Collaboration), arXiv:1105.1806v1, submitted in Phys. Rev. D.
- [10] T. Aaltonen et al. (CDF Collaboration), Phys. Rev. D **81**, 052001 (2010).
- [11] A. Bhatti, et al., Nucl. Instrum. Methods Phys. Res. A **566**, 375 (2006).
- [12] T. Sjostrand, S. Mrenna, and P. Skands, J. High Energy Phys. 05 (2006) 026.
- [13] G. Bevilacqua, et al., J. of High Energy Phys. 09 (2009) 109.
- [14] T. Junk, CDF public note 8128; T. Junk, Nucl. Instrum. Methods in Phys. Res. A **434**, 435 (1999).